IHJPAS. 35(4)2022

Ibn Al-Haitham Journal for Pure and Applied Sciences

Journal homepage: http://jih.uobaghdad.edu.iq/index.php/j/index

Producing Hydrogen Energy Using Cr_2O_3-TiO_2 Nanocomposite with Animal (Chitosan) Extract via Photocatalysis

Ghasaq Z.Alwan
Department of Physics, College of Education Mustansiriyah University, Baghdad, Iraq.
Gasaq.zuher@gmail.com

Wisam J. Aziz
Department of Physics, College of Education Mustansiriyah University, Baghdad, Iraq.
wisamjafer14@gmail.com

Raad S. Sabry
Department of Physics, College of Education Mustansiriyah University, Baghdad, Iraq.
raadsaadon74@gmail.com

Article history: Received 8 May 2022, Accepted 14 June 2022, Published in October 2022.

Doi: 10.30526/35.4.2853

Abstract

In this study, an efficient photocatalyst for water splitting was developed. The Cr_2O_3 and TiO_2 nanoparticles (Cr_2O_3-TNPs) nanocomposite with (Chitosan extract) was created using ecologically friendly methods, such as the impregnation technique as TiO_2 exhibits nano spherical (TNPs) shape structure. According to the researchers, this nanocomposite material enhanced its ability to absorb ultraviolet light while also speeding up the recombination of photogenerated electrons and holes. The TNPs and prepared Cr_2O_3-TNPs were characterized by X-ray diffraction (XRD), field emission scanning electron microscopy (FE-SEM), energy dispersive x-ray spectroscopy (EDX), and UV-visible absorbance. The XRD of TNPs showed a Tetragonal phase with 8.9 nm of average crystallite size and 14.2 nm for nanocomposite. FE-SEM images showed that the average particle size in the range of (12.5-57.5) nm and UV-VIS absorbance has energy gap of 3.8 eV, while the energy gap of Cr_2O_3-TNPs is 2.8 eV. It was found that the performance of photocatalysts of the nanocomposite for hydrogen generation was superior. It gave the highest rate of hydrogen production (3.6) ml at 80 min when exposed to ultraviolet light. Moreover, the nanocomposite revealed high H_2 production rate under ultraviolt light irradiation ($\lambda < 400$ nm). The Cr_2O_3-TNps have high photocatalytic effectiveness due to their wide ultraviolt light photoresponse range and excellent separation of photogenerated electrons and holes.

Keywords: Cr_2O_3-TNPs nanocomposite; chitosan extract; hydrogen production; photocatalyst.

1. Introduction

Hydrogen has the potential to be a powerful energy carrier and an appropriate energy storage material to substitute fossil fuels, a wealth of natural resources such as biomass and water [1][2]. Photocatalytic water splitting, in particular, is being investigated as a possible approach for producing hydrogen using solar light [3]. Various inorganic or organic semiconductors have been explored over the last 40 years. However, it has primarily been used in the water splitting half-reaction example as the oxidation of water to oxygen (O_2) or the reduction of protons to hydrogen (H_2)[4][5]. The limitations of water splitting in pure water over a semiconductor are limited effective separation of photogenerated carriers and the rapid H_2-O_2 recombination reverse reaction [6][7]. In this case, photocatalysis is a viable method for producing hydrogen because it can utilize solar energy in a cost-effective and environmentally friendly process while also being more cost-effective than traditional methods. However, society not only provides comfort and well-known technology but also comes with the well-known disadvantage of CO_2 release. Most combustion activities produce this gas, which is thought to be the primary cause of global warming since global industrialization has risen by a significant amount [8].

Hydrogen widely believed to be the most potential clean energy carrier for the future and whose usage is being researched in many technology sectors, is an appealing alternative to fossil fuels as an energy source [9]. Water is a natural source of hydrogen and oxygen, and over the last few decades been a surge in interest in using photocatalysis to split water and make H_2 [10]. In photocatalysis, TiO_2 is the most commonly used semiconductor because of its physical and chemical qualities, as well as its wide availability, outstanding stability, inexpensive cost [11], alternation of the surface [12][13], co-catalysts for loading [14][15], heterojunctions creation [16][17] .The photocatalytic process involves photon excitation of a semiconductor to generate electron-hole pair (of appropriate energy - higher or equal to the band gap). Electrons and holes recombine or migrate to the surface of the semiconductor particle, where reduction and oxidation reactions occur. A semiconductor with a conduction band more negative than the H_2O/H_2 redox couple (0.0 V) and a valence band more positive than the O_2/H_2O redox couple is required for H2 generation by water splitting (1.23 V versus NHE) at pH = 0. TiO_2 (band gap 3.0-3.3 eV) is the semiconductor with the most potential for creating hydrogen from water or biofuels. However, the semiconductor with the most potential for creating hydrogen is biofuels or water. Bare TiO_2 is ineffective in producing hydrogen.

It is often attributed to high hydrogen over potential caused by rapid electron-hole recombination. TiO_2 has been modified with transition-metal cations to increase its absorption capacity for light and its photocatalytic capabilities [18][19]. Cr_2O_3 is generally considered an excellent photocatalytic material for ultraviolet light because of its tight band gap; thus, it has been considered a TiO_2 dopant [19][20]. Cr^{3+} was mixed into TiO_2 powder to increase its photocatalytic capabilities [21]. Several studies have suggested adding chromium oxide to titanium oxide and improving the effectiveness of photocatalysis [22]. In this study, chromium oxide (Cr_2O) with animal (chitosan) extract was loaded on titanium oxide (TiO_2) to obtain a Cr_2O_3-TiO_2 nanocomposite using the impregnation technique. It is possible to detect some of the essential constituents in the animal extract (chitosan), including preliminary totals found in the rutin (Rutin is a rutinoside that is quercetin with the hydroxy group at position C-3 replaced by glucose and rhamnose sugar groups) vitamin C.

Cellulose is also included in chitosan, a significant component of the chitosan extract [23]. Animal extract (chitosan) was used to synthesize Cr_2O_3-TiO_2. The OH team has a significant impact on

reduction. To reduce $Cr(NO_3)_3$ hydroxide, chitosan extract partially reduces $Cr(NO_3)_3$ hydroxide to generate Cr_2O_3-TiO_2 nanocomposite. This work aims to synthesize the Cr_2O_3-TiO_2 nanocomposite to improve photogenerated electron-hole pair efficiency and photocatalytic activity by improving optical responsiveness in the ultraviolet range.

2. Materials and Methods

2.1. Preparation of the Animal Extracts (chitosan)

0.5 gm. of chitosan was dissolved in 1:50 acetic acid with water ratio and ultrasonically mixed for 2 h, then filtered using a micro porous membrane (pore size. Mm) and cleared several times by the centrifuge at 4000 rpm for 5 minutes to remove any residual salts and impurities.

2.2. Preparation of the Cr_2O_3-TiO_2 nanocomposites

Cr_2O_3-TiO_2 nanocomposite was synthesized using 0.0329 gm. of Cr $(NO_3)_3.9H_2O$ with 2 ml from anhydrous ethanol solution and 1 ml of chitosan extract treated with ultrasonic assistance to produce a clear dark blue solution that was then impregnated with 2.5 gm. Commercial TiO_2 nanoparticles were purchased from Sky spring Nanomaterial. The impregnate was volatilized at 70°C until being annealed for 2 hours at 300°C.

2.3. Characterization of Cr_2O_3-TiO_2nanocomposites

Characterization of TiO2 nanoparticls (TNPs), and Cr_2O_3-TNPs were carried out by different techniques. UV–visible spectrophotometer type (DU- 8800D- China) within the range (190-1100) nm. The morphological properties was examined used Field Emission Scanning Electron Microscopy (FESEM INSPECT F-50, Company FEI, Dutch) with energy dispersive (X-Ray) spectroscopy (EDX). X-Ray diffraction was recorded with a SHIMADZU (XRD-6000, JAPAN) using CuKα radiation (λ=1.5406 Å).

2.4. The Assessment of Photocatalytic Hydrogen Generation

As shown in figure 1, the laboratory cell used to separate hydrogen from the water was made locally from a hydrogen gas cylinder quartz glass (6cm x 28cm). The cylinder is equipped with holes for the exit of gas. Water decomposition was carried out using an analytical system, such as the quantity of photocatalysts. 2 gm of Cr_2O_3/TiO_2 placed in a quartz flask containing (500 ml) water and 0.028 M of KOH of a sacrificial reagent aqueous solution (Cr_2O_3-TiO_2) which exposed using ultraviolet light irradiation (λ<400nm).

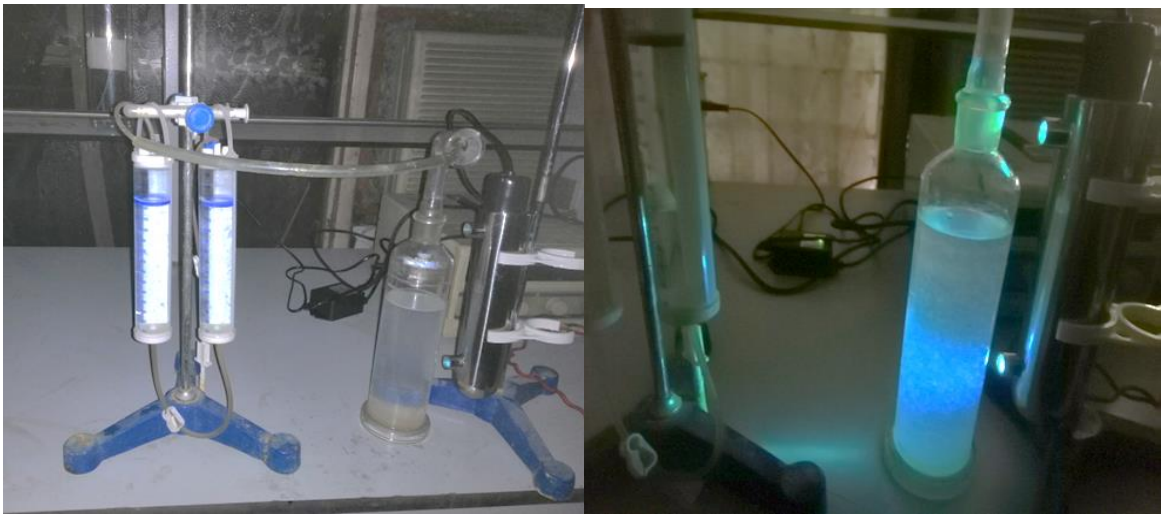

Figure 1: Laboratory hydrogen separation system.

3. Results and dissection

3.1 XRD analysis

The XRD pattern of TNPs reveals the planes (101), (103), (004), (112), (200), (105), (211), (204), and (116) assigned at 2θ of (24.8°), (36.9°), (37.8°), (38.3°), (48.2°), (53.7°), (55.2°), (62.6°), and (68.2°), respectively as shown in figure 2. The diffraction peaks reveal a tetragonal anatase phase, according to (JCPDS No. 84-1285). The strongest diffraction peak at 24.8° indicated to (101) plane of anatase TiO_2, The anatase structure is responsible for the peaks other than (53.7°) and (55.2°), while the rutile structure is also responsible for the peaks (53.7°) and (55.2°). This indicates that anatase is the dominant crystal phase in TiO_2 nanoparticles, with the presence of some rutile phases in small amounts in the final product. These findings are consistent with earlier research by[24]. The average crystallite size, founded by Scherer's formula [22], equals to 8.9 nm of TNPs.

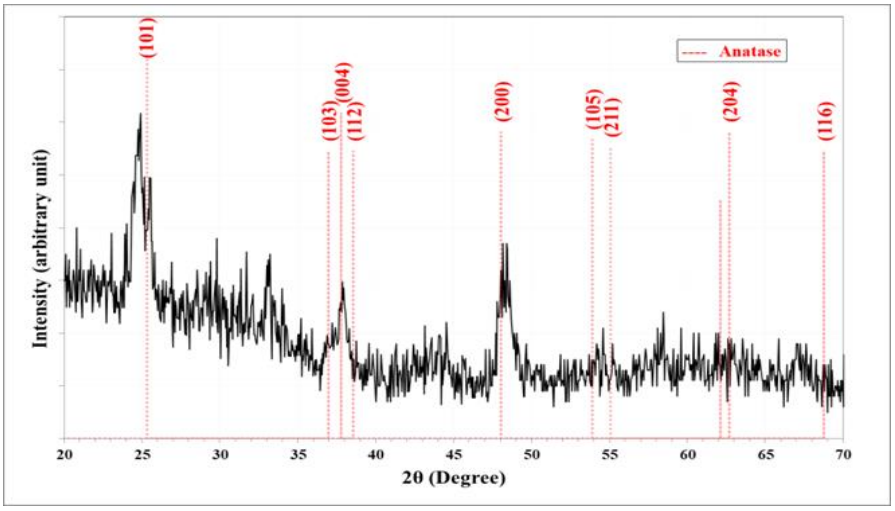

Figure 2.XRD patterns of TNPs

Figure 3 illustrates the XRD spectra of Cr_2O_3-TNPs nanocomposite heterostructures at different Cr_2O_3 percentages. Diffraction planes (101), (104), (103), (004), (112), (202), (200), (105), (211), (204), and (116) (JCPDS Card NO. 84-1285), corresponding to 2θ = (24.7°),(36.5°),(37.8°), (38.1°), (47.9°), (53.8°), (55.5°), (62.7°) and (68.5°) are seen in the crystallized anatase phase of Cr_2O_3-TNPs. Because of the small proportions of Cr_2O_3 particles relative to the TiO_2 ratio, the XRD result appears the tiny peaks of Cr_2O_3 at 2θ = (33.1°) and (44.2°) (JCPDS No. 1308-38-9). According to these findings, the successful modification of titanium dioxide with the amount of Cr_2O_3 has created flaws in the anatase crystal to form Ti-O-Cr bonds which allow it to interact with both Cr^{3+} ions and TiO_2. As a result, it is concluded that the presence of Cr2O3 blocks the pore wall of TiO2.The crystal size of Cr_2O_3-TNps is 14.2 nm.

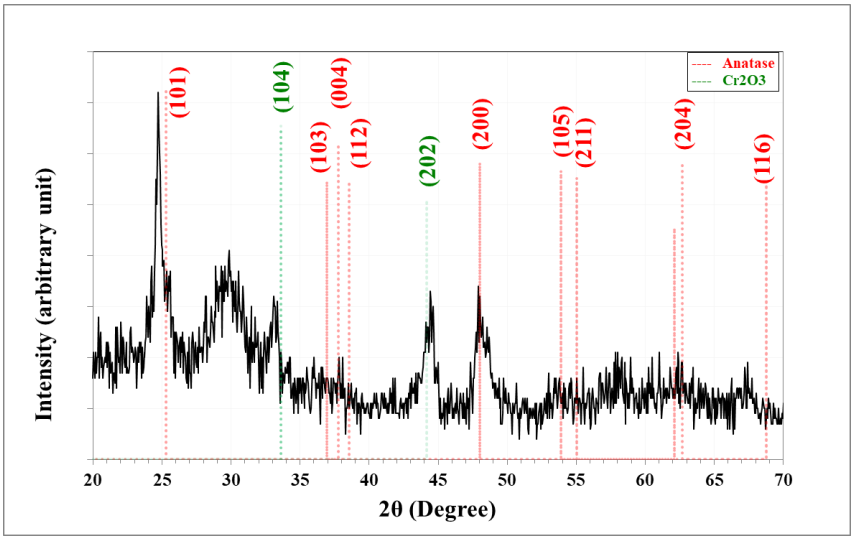

Figure 3. XRD patterns of Cr_2O_3-TNPs nanocomposites.

3.2 FE-SEM images ofTNPs and Cr_2O_3-TNPsnanocomposites

The morphology of TNPs in figure (4-A) appears as semi-spherical, with an average particle size of 12.5-57.5 nm (measured using Image J software). Figure (4-B) shows Cr_2O_3 with TNPs where exhibited the agglomeration of nanoparticles and the formation of a wide surface area [25], where the bonding of chromium and titanium oxide particles by weak forces led to these agglomerations.

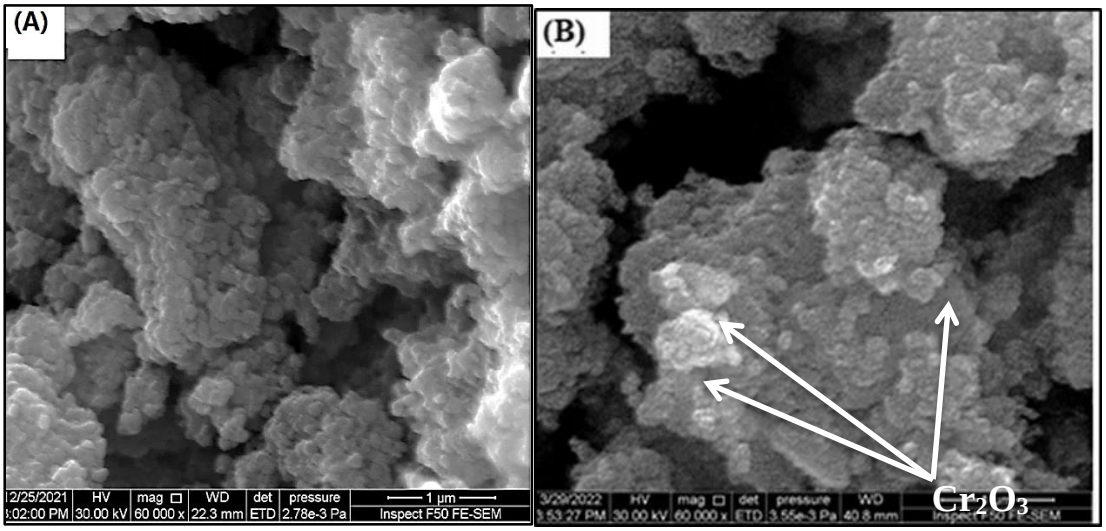

Figure 4. FE-SEM images of (A) TNPs.(B)Cr_2O_3 -TNPs composite

3.3.EDX of of TNPs and Cr_2O_3-TNPs nanocomposites

EDX analyses of TNPs and Cr_2O_3 with TNPs nanocomposite are shown in Figure 5 and Table 1. It reveals the characteristic emission peaks for Ti and O_2, in addition to C and some trace elements observed in both samples as a residual that comes from the extracted material. The presence of phytomolecules (polyphenols, alkaloids, and flavonoids) of chitosan is extracts adsorbed on the TNPs surface.

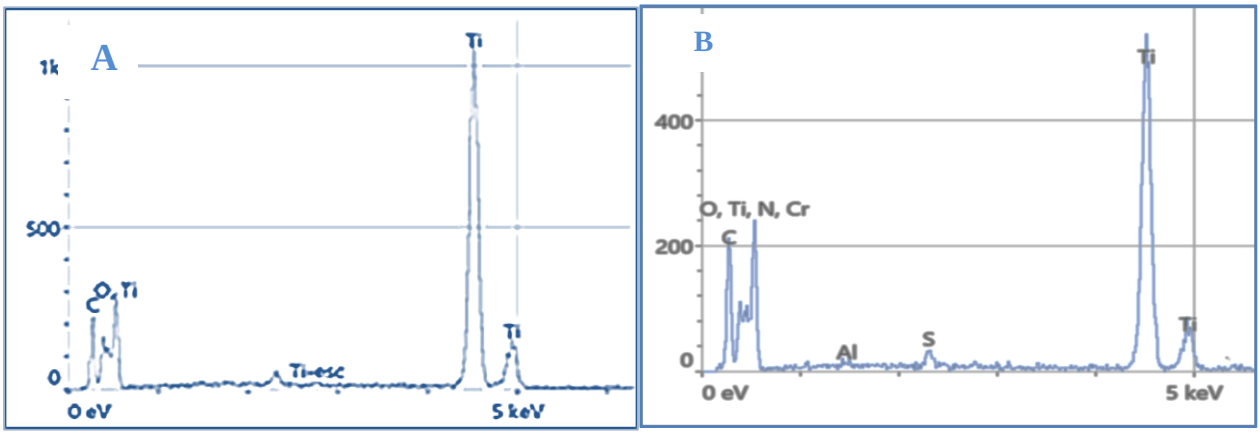

Figure 5. The elements, atomic and weight ratios of (A) TNPs (B) Cr_2O_3 with TNPs nanocomposite with Chitosan

Table 1. The elements, atomic and weight ratios of TNPs and Cr_2O_3 with TNPs

Element	TNPs		Cr_2O_3 with TNPs	
	Atomic %	**Weight %**	**Atomic%**	**Weight %**
O	18.0	41.5	49.9	45.8
Ti	57.3	44.2	9.0	31.7
C	24.7	14.3	34.9	19.0
Cr	_____	_____	0.1	0.4
S	_____	_____	0.3	0.6
N	_____	_____	5.9	2.5

3.4 Ultraviolet Visible (UV-Vis)

Figure 6 depicts the UV-visible absorption spectra of samples where the TNPs sample absorption edge is located at 300 nm. The Tauc formula was used to determine the energy gap equal to 3.8 eV for the TNPs, as shown in **Figure 7**.

Figure 8 shows that Cr^{3+} loading into TNPs improves their absorption in the UV-Visible region, the absorption edge of Cr_2O_3-TNPs appears at 415 nm, and the energy gap is equal to 2.8 eV, as shown in figure 9. The absorption edge of the Cr_2O_3-TNPs nanocomposite with chitosan extract shifted to a greater wavelength in the visible region as compared to the undoped TNPs. It may be concluded that proper Cr doping resulted in the anatase TiO_2 band gap narrowing. The introduction of dope levels is to cause a narrower band gap. This would also cause an electron to be excited from the valence band to the dope levels. Cr doping may also act as an electron-capture trap, preventing the recombination of electron-hole pairs. On the other hand, Cr doping produces deep dope levels and recombination sites that can speed up the recombination of electron-hole pairs [26].

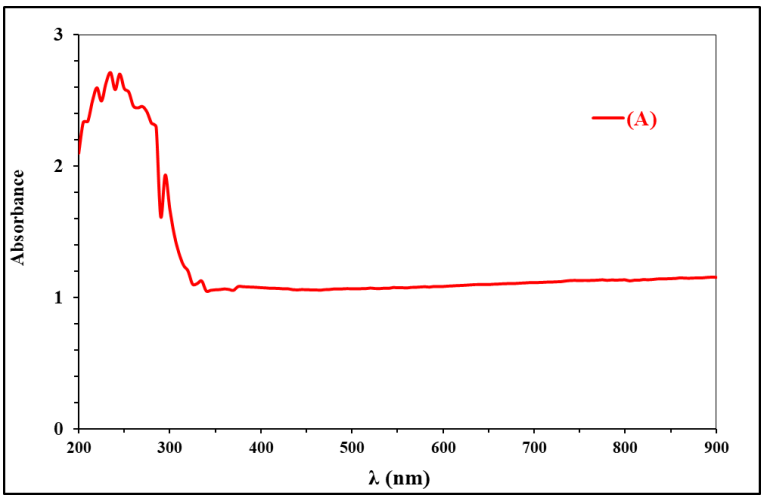

Figure 6. Ultraviolet-visible absorption spectra of TNPs.

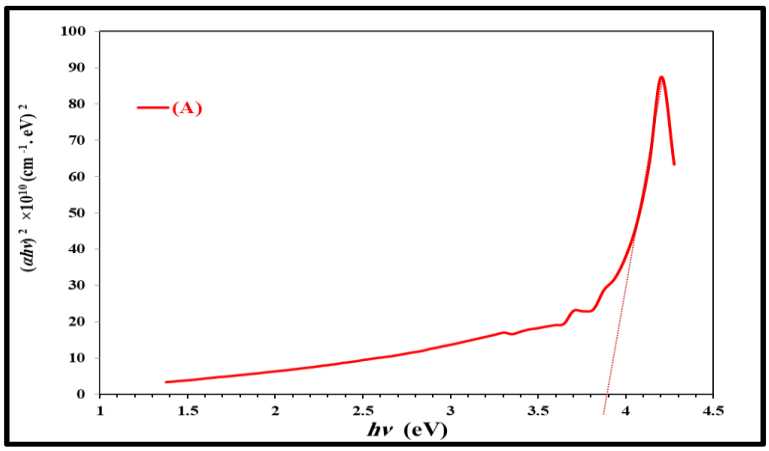

Figure 7. The energy gap of TNPs**.**

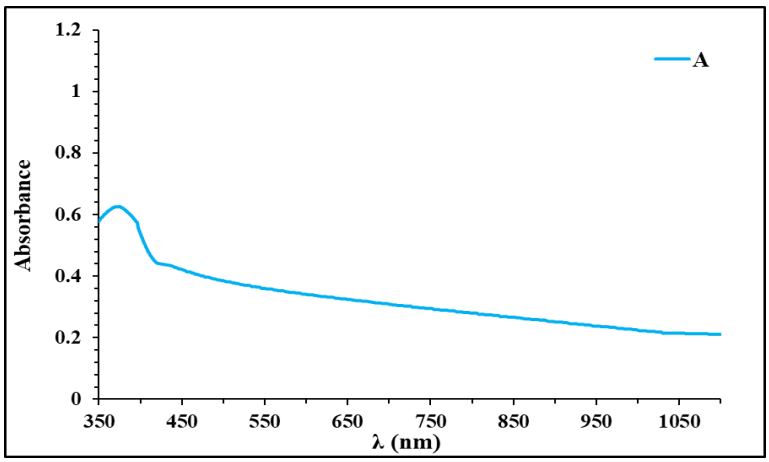

Figure 8. Ultraviolet-visible absorption spectra of Cr_2O_3-TNPs nanocomposite

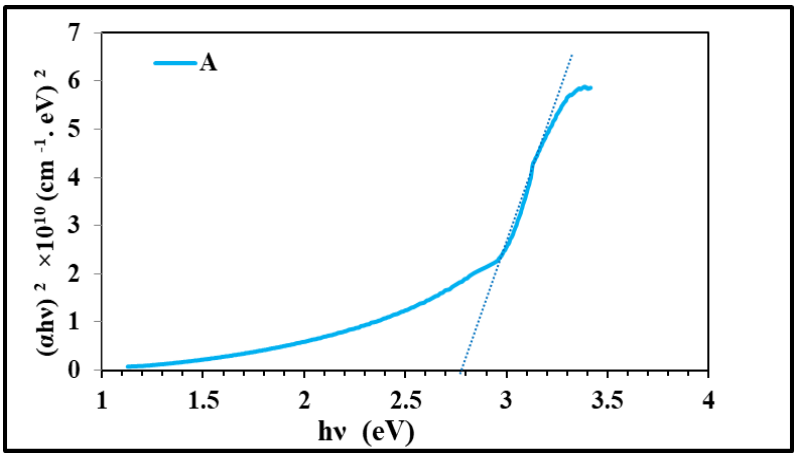

Figure 9. The energy gap of Cr_2O_3-TNPs.

3.5. Activity of hydrogen production

The photocatalytic decomposition of water under ultraviolet light irradiation generated hydrogen for Cr_2O_3 –TNPs. The average hydrogen generation for Cr_2O_3-TNPs at different times (10 - 80) min are summarized in **Figure (10) and Table (2)**, it was observed that the hydrogen was not produced in the first 10 min of the reaction. The lowest hydrogen production was (0.2) ml at 20 min and the highest hydrogen production at 80 min was (3.6) ml. The effectiveness of the components (such as salts and oxides of transition metals) for many catalysts is spontaneously dispersed on the surface of the carriers, where hydrogen gas is produced in a volume twice the size of oxygen gas through as well as the photocatalyst, an increase in hydrogen production was observed due to the effect photocatalysts on the reaction speed. The work of the photocatalyst must comply with many basic principles to obtain an efficient hydrogen production process, meaning that the best photocatalyst for hydrogen production is the one with the highest quantitative yield and the highest gaseous production rate. The main measure of photocatalyst action is quantitative.

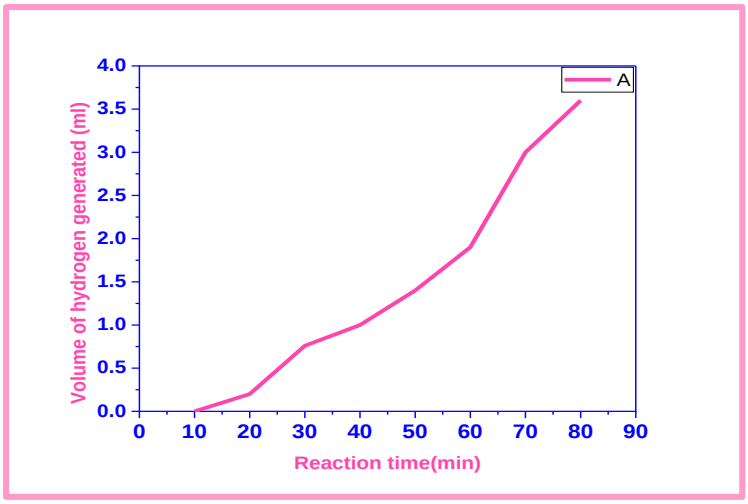

Figure (10). Time courses of hydrogen evolution over Cr_2O_3-TNPs with chitosan extract.

Table (2). Volume of hydrogen generated (ml) and reaction time of (Cr_2O_3-TNPs).

Cr_2O_3-TNPs Volume of hydrogen generated (ml)	**Reaction time(min)**
0	10
0.2	20
0.76	30
1.0	40
1.4	50
1.9	60
3.0	70
3.6	80

5. Conclusion

Impregnation processes were used to create Cr_2O_3-TiO_2 nanocomposites. XRD and FESEM analysis of nanocomposites showed that they contained a mixture of Cr_2O_3-TiO_2 (nanospherical). The average diameter of the nanospherical was (12.5-57.5) nm. The absorption edge of TNPs can be extended to the ultraviolet range was 300 nm, and the energy gap is equal to 3.8 eV is larger than the energy gap of Cr_2O_3-TNPs is equal to 2.8eV because the appropriate Cr doping resulted in a narrowing of the band gap of the anatase TiO_2. Briefly, it has succeeded in synthesizing environmentally friendly biomolecules via the impregnation route. If the effect of the morphology of the compound Cr_2O_3-TNPs was in the form of spherical, it was discovered to have an effect on the performance of the current work, where the compound Cr_2O_3-TNPs showed a distinguished performance in hydrogen production through photocatalysts and increased with increasing time, the highest production at the 80 min, it was (3.6) ml. We conclude from the above that the nanocomposite's ability to make hydrogen largely depends on the amount of Cr3+ that can be added to the TNPs.

References

1.Gray, H. B.; Powering the planet with solar fuel. *Nat Chem.* **2009**. 1: 7–17

2.Tian,B.; Gao, W.; Zhang, X.; Wu, Y.; and Lu, G.; Water splitting over core-shell structural nanorod CdS@Cr2O3 catalyst by inhibition of H2-O2 recombination via removing nascent formed oxygen using perfluorodecalin, *Appl. Catal. B Environ*, **2017.** 221, 618–625, doi: 10.1016/j.apcatb.09.065.

3.Osterloh, F. E.; Inorganic materials as catalysts for photochemical splitting of water, *Chem. Mater.* **2008.** 20, 1, 35–54.

4.Tian, B.; Zhen, W.; Gao, H.; Zhang, X.; Li, Z. and Lu, G. Carboxyl-assisted synthesis of Co nanorods with high energy facet on graphene oxide sheets for efficient photocatalytic hydrogen evolution," *Appl. Catal. B Environ.*, **2017.** 203, 789–797.

5.Meng, X.; Li, Z.; Zeng, H.; Chen, J.; and Zhang, Z.; MoS_2 quantum dots-interspersed Bi2WO6 heterostructures for visible light-induced detoxification and disinfection, *Appl. Catal. B Environ.*, **2017.** 210, 160–172,

6.Jia, L. D.; Wang, H. Y.; Huang, X. A.; Xu, W.; and Yu, H. Q.; Highly durable N-doped graphene/CdS nanocomposites with enhanced photocatalytic hydrogen evolution from water under visible light irradiation, *J. Phys. Chem. C*, **2011.** 115, 23, 11466–11473,

7.Tian, B.; Water splitting by CdS/Pt/WO3-CeOx photocatalysts with assisting of artificial blood perfluorodecalin," *J. Catal.*, **2017.** 350, 189–196,

7.Caetano, M. A.; Gherardi, D. F.; and Yoneyama, T.; Optimal resource management control for CO2 emission and reduction of the greenhouse effect, *Ecol. Modell.*, **2008.** 213, 1, 119–126.

9.Rand, D. A.; and Dell, R. M.; *Hydrogen energy: challenges and prospects*. *Royal Society of Chemistry*, **2007.** 2. 45.

10.Bahruji, H.; Sustainable H2 gas production by photocatalysis, *J. Photochem. Photobiol. A Chem.*, **2010.** 216, 2, 115–118.

11.Schneider, J.; Understanding TiO2 photocatalysis: mechanisms and materials, *Chem. Rev.*, **2014.** 114, 19, 9919–9986,

12.Wang, H.; Hu, X.; Ma, Y.; Zhu, D. ; Li, T.; and Wang, J. ; Nitrate-group-grafting-induced assembly of rutile TiO2 nanobundles for enhanced photocatalytic hydrogen evolution, *Chinese J. Catal*. **2020.** 41, 1, 95–102,

13.Wang, P.; Xu, S.; Chen, F.; and Yu, H.; Ni nanoparticles as electron-transfer mediators and NiSx as interfacial active sites for coordinative enhancement of H2-evolution performance of TiO2, *Chinese J. Catal.*, **2019.** 40, 3, 343–351.

14.Shen, J. ; Wang, R.; Liu, v; Yang, X.; Tang, H.; and Yang, J.; Accelerating photocatalytic hydrogen evolution and pollutant degradation by coupling organic co-catalysts with TiO2, *Chinese J. Catal.*, **2019.** 40, 3, 380–389,

15.Meng, A.; Zhang, L.; Cheng, B.; and Yu, J.; Dual cocatalysts in TiO2 photocatalysis, *Adv. Mater.*, **2019.** 31, 30, 1807660,

16.Li, H.; Zhou, Y.; Tu, W.; Ye, J.; and Zou, Z.; State-of-the-art progress in diverse

heterostructured photocatalysts toward promoting photocatalytic performance, *Adv. Funct. Mater.*, **2015.** 25, 7, 998–1013,

17.Zhang, W.; Zhang, H.; Xu, J.; Zhuang, H.; and Long, J.; 3D flower-like heterostructured TiO2@ Ni (OH) 2 microspheres for solar photocatalytic hydrogen production, *Chinese J. Catal.*, **2019.** 40, 3, 320–325,

18.Wang B.; Cr2O3@ TiO2 yolk/shell octahedrons derived from a metal–organic framework for high-performance lithium-ion batteries, *Microporous Mesoporous Mater.*, **2015.** 203, 86–90,

19.Huang H.; Design of twin junction with solid solution interface for efficient photocatalytic H2 production, *Nano Energy*, **2020.** 69, 104410,

20.Mao, G.; Xu, M.; Yao, S.; Zhou, v; and Liu, Q. ; Direct growth of Cr-doped TiO 2 nanosheet arrays on stainless steel substrates with visible-light photoelectrochemical properties, *New J. Chem.*, **2018.** 42, 2, 1309–1315,

21.Ahmad, M. M.; Mushtaq, S.; Al Qahtani, H. S.; Sedky, A.; and Alam, M. W.; Investigation of TiO2 Nanoparticles Synthesized by Sol-Gel Method for Effectual Photodegradation, Oxidation and Reduction Reaction, *Crystals*, **2021.** 11, 12, 1456,

22.Tsegay, M. G. Gebretinsae, H. G. and Nuru, Z. Y.; Structural and optical properties of green synthesized Cr2O3 nanoparticles, *Mater. Today Proc.*, **2021.** 36, 587–590,

23.Bharathi, D.; Ranjithkumar, R.; Vasantharaj, S.; Chandarshekar, B.; and Bhuvaneshwari, V.; Synthesis and characterization of chitosan/iron oxide nanocomposite for biomedical applications, *Int. J. Biol. Macromol.*, **2019.** 132, 880–887,

24.Behnajady, M. A.; Eskandarloo, H.; Modirshahla, N. ; and Shokri, M. ; Investigation of the effect of sol–gel synthesis variables on structural and photocatalytic properties of TiO2 nanoparticles, *Desalination*, **2011.** 278, 3, 10–17,

25.Alzahrani, K. A.; Mohamed, R. M.; and Ismail, A. A.; Enhanced visible light response of heterostructured Cr2O3 incorporated two-dimensional mesoporous TiO2 framework for H2 evolution, *Ceram. Int.*, **2021.** 47, 15, 21293–21302,

26.Zhu, H.; Tao, J.; and Dong, X.; Preparation and photoelectrochemical activity of Cr-doped TiO2 nanorods with nanocavities, *J. Phys. Chem. C*, **2010.** 114, 7, 2873–2879,